The Dynamic Scattering Coefficient on Image Dehazing Method with Different Haze Conditions

Noor Asma Husain(✉) and Mohd Shafry Mohd Rahim

School of Computing, Faculty of Engineering, Universiti Teknologi Malaysia, Johor Bahru, Malaysia
nasma4@live.utm.my, shafry@utm.my

Abstract. The dust, mist, haze, and smokiness of the atmosphere typically degrade images from the light and absorption. These effects have poor visibility, dimmed luminosity, low contrast, and distortion of colour. As a result, restoring a degraded image is difficult, especially in hazy conditions. The image dehazing method focuses on improving the visibility of image details while preserving image colours without causing data loss. Many image dehazing methods achieve the goal of removing haze while also addressing other issues such as oversaturation, colour distortion, and halo artefacts. However, some of the approaches could solve these problems and be effective at a certain level of haze. A volume of various haze level data is required to demonstrate the efficiency of the image dehazing method in removing haze at all haze levels and obtaining the image's quality. This study proposed a new dataset by simulating synthetic haze in images of outdoor scenes. The synthetic haze simulation is based on the meteorological range and works on specific haze conditions. In addition, this paper introduced a dynamic scattering coefficient to the dehazing algorithm to determine the appropriate visibility range for different haze conditions. These proposed methods improve on the current state-of-the-art dehazing method in terms of image quality measurement results.

Keywords: Haze · Scattering coefficient · Image dehazing · Atmospheric scattering model

1 Introduction

Air pollutants such as dust, sand, water droplets or ice crystals are responsible for the phenomenon of haze, fog, and mist atmospheric. These weather phenomena mainly differ in material, size, shape, and concentration. The haze seems to create a clear grey or blue hue and decreases visibility [1]. The haze of outdoor images is an estimated degradation, especially in computer visions, where the image contrast decreases when the light is scattered in particulate matter suspended. This causes low contrast and poor image visibility. The lack of details caused by haze makes images visually unattractive

Z. Lv and H. Song (Eds.): INTETAIN 2021, LNICST 429, pp. 223–241, 2022.
https://doi.org/10.1007/978-3-030-99188-3_14

and presents human and engine vision challenges, which restrain the identification, tracking or navigation of objects [2, 3].

The contributions control the optical thickness of the medium between the camera sensor and the captured object. Scattering and absorption reduce direct transmission from the image to the camera, creating another layer of ambient scattered light, known as air-light, as seen in Fig. 1. Koschmieder [4] proposed a haze-explained atmospheric scattering model in which poor image quality was caused by horizontal airlight dispersion and reflection, as well as propagation-based attenuation. Due to the attenuated direct transition, the scene's strength is diminished, and the scene's appearance is washed out due to the airlight. Earlier research has shown considerable improvement in approaches that use hazy images. Nayar and Narasimhan [1] estimate their depth, Cozman and Krotkov [5], with the use of atmospheric signals. Since then, many explicit methods have been established for enhancement of visibility and can be broken down into four categories: multi-picture methods [6], filter-based methods [7], proven depth or geometry methods [8] and single-picture methods. [9, 19].

Most of the dehazing single-image algorithms recently introduced different approaches to restoring the hazy look to a natural hazel-free image. Researchers have developed different methodologies on the same principle to retrieve the clean scene from the haze. An accurate medium of the transmission map is the primary purpose. The results of Tan [9] and Fattal [10] improved visibility for one image and automatically eliminated haze in a single image without further information, for example, known geometric information or user feedback. One of the system's drawbacks is the presence of a halo around the depth discontinuity due to local window activity. In his early investigation, Tan [9] received a less reliable estimate. Fattal [10] only functions successfully at low haze and its output decreases at medium and high haze. Fattal [15] proposes another approach based on colour lines but with low brightness. He et al. [11] and his colleagues discovered that most outdoor items have at least one colour channel significantly dark in clear weather. One of the techniques' drawbacks is their computational time, especially in real-time applications where the depth of the input scenes varies from frame to frame. Tarel and Hautiere [12] introduce a fast visibility restoration method with a complexity that is linear to the number of image pixels.

Meng et al. [13] expand the concept of the dark channel by introducing the lower limit before defining the initial transmission values. The transmission of He et al. [11], Meng et al. [13] is also a bit underestimated because the lower transmission boundary is essentially predicted. Estimates from He et al. [11] and Meng et al. [13] become more accurate with the increase in the haze. Ancuti proposes a colour distortion method for image fusion [14]. Tang et al. [16] provide a learning framework. The random forest regressor is used to learn how to associate the features with the transmission. The process yields multi-scale characteristics such as dark channel, maximum local contrast, hue disparity, and maximum regional saturation. Zhu et al. [17] propose Color Attenuation Prior (CAP), which is based on the difference between the saturation and brightness of the hazy image pixels. By using colour attenuation for model parameters to estimate the transmission depth prior to a supervised learning process. Cai et al. [18] propose a learning-based system in which a regressor is trained to predict the value of the transmission from its surrounding patch. The learning techniques, however, rely heavily on the white balancing stage with proper light colour. If minor mistakes in environmental colour measurements arise, their output decreases rapidly. Berman et al. [19] proposes a non-local prior algorithm. Berman makes a minor estimation error at medium hazards, but the error increases at low and heavy haze. Earlier research investigated the problems that were discovered when dealing with haze at various levels. Some of the approaches did not cater to dense haze levels or low haze levels [11, 19]. As a result, it emphasises the significance of image dehazing assessment at various haze levels. A dataset volume is required to meet this requirement to evaluate the efficiency of the image dehazing method in removing haze at all haze levels.

Although many algorithms are proposed for image dehazing, there are insufficient proven criteria or benchmarks for the evaluation of different haze levels. Six datasets for objective analysis algorithm were proposed in the works in advance: FRIDA [20], D-hazy [21], CHIC [22], HAZERD [23], O-HAZY[23] and I-HAZY [25]. FRIDA is highly specialised and presents numerous synthetic hazy road images from the driver's perspective. Indoor scenes not characteristic of the traditional dehazing programme, D-hazy uses depth images from Middlebury [26] and NYU depth V2 [27]. CHIC utilises a fog machine in an indoor setting and offers two indoor scenes with known objects and two scenes with window-viewed outdoor content.

This paper proposes a new dataset that simulates synthetic haze at four different levels based on the meteorological range, as shown in Table 2. The aim is to identify haze level in various atmospheric conditions [28, 29]. The datasets could evaluate the efficiency of future image dehazing to remove haze at any levels. Therefore, this paper also proposes the enhancement dehazing method with a dynamic scattering coefficient to improve the quality of the image in different atmospheric conditions.

Table 1. Haze databases.

Year	Method	Scene	Depth-based
2012	FRIDA [20]	Outdoor	Free-Space Segmentation (FSS)
2016	DHAZY [21]	Indoor	Stereo image
2016	CHIC [22]	Indoor	Actual distance
2017	HAZERD [23]	Outdoor	Fusing structure from motion and lidar
2018	IHAZY [25]	Indoor	Stereo images
2018	OHAZY [24]	Outdoor	Stereo images
2020	VHAZE* [29]	Outdoor	Actual distance

* *Our dataset*

2 Atmospheric Scattering Model

The atmospheric scattering model proposed by Koschmieder [4] has two mechanisms, which are direct attenuation, $J(x)\ t(x)$, and air-light, $A(1-t(x))$, as shown in Fig. 1.

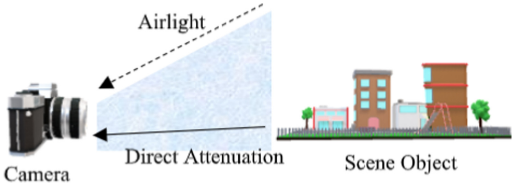

Fig. 1. Atmospheric Scattering phenomena

Haze algorithm combined these mechanisms, given by [3], as follows:

$$I(x) = J(x)t(x) + A(1 - t(x)) \tag{1}$$

where *I(x)* is the haze image, *J(x)* is the haze-free image, *t(x)* is direct transmission, and *A* is the air-light. In early work, the most haze-opaque pixel was used to estimate air-light. Tan [9] chose the brightest pixel. Fattal [10] used it as an initial guess for an optimization query. The pixels with the highest intensity can be bright object instead of air-light. He et al. [11] states that the brightest pixel should be chosen between the pixels of the darkest channel with the highest brightest values. This is a functional method that generates reliable results. The most difficult part is to estimate the transmission maps *t(x)* between the lightning of the camera and the scene. Distance, *d(x)* from the camera observer is the point of the scene. The transmission of haze is physically associated with depth has been observed. Depth assessment is a major yet computer vision challenge [30].

$$t(x) = e^{-\beta d(x)} \tag{2}$$

For calculation of direct transmission, the atmospheric scattering component, β, distance or depth of the scene, *d(x)*, between the observation and the target object are used. It should be noted that the scene's depth is the most important information [4]. Since the scattering coefficient can be regarded as a constant homogenous state of the atmosphere, the medium transmission, *t(x)*, can easily be calculated with Eq. (2) if the depth is known. *t(x)* in the scalar [0,1] represents a transmission map. Some issues, such as halo artefacts, may result in an incorrect transmission map estimate. Once the air-light and transmission map has been calculated, the hazy image, *J(x)*, can be restored to a haze-free appearance using Koshmieder's [4] Eq. (3):

$$J(x) = \frac{I(x) - A}{t(x)} + A \tag{3}$$

Equation (3) illustrates the formula from Eq. (1) for restoring a hazy image using estimated transmission and air-light. Most dehazing approaches used this formula, and instead of directly using the scattering coefficient, they proposed various techniques to obtain a transmission map. This paper improved the dehazing method by incorporating a dynamic scattering coefficient into our methodology, detailed in the following section.

3 Methodology

This section explains the research framework in Fig. 2 for the proposed dehazing algorithm. The haze simulation is determined using the model of atmospheric scattering in

Eq. (1). To get a haze image, $I(x)$ it requires a haze-free image, $J(x)$, air-light value, A and transmission value, $t(x)$. The default RGB value of an air-light is set to [1, 1, 1]. A clear image with a known distance $d(x)$ between the camera and the target is captured. The scattering coefficient is derived based on the captured distance map. Then it will calculate the transmission map value as in Eq. (2). Based on the air pollutant index and environmental conditions, the picture taken must be on a clear day to be classified as a haze-free image. The synthetic haze images were simulated in a clear image, which referred to the meteorological range [30]. The simulation creates four different haze conditions in a haze-free image.

This dehazing algorithm is primarily calculated by using Eq. (1) to apply the atmospheric scattering model. This process of pre-processing employs gamma correction on the hazy input image. Next, quadtree decomposition estimates air-light based on the corrected image brightness [31]. Following that, the scene depth estimated with Dark Channel Prior is used to compute haze thickness [11]. Based on the estimated scene depth, we compute the mean value to obtain the appropriate scattering coefficient value, β, based on the visibility range of the hazy image. Estimation of the visibility range uses a new visibility scale within the intensity range [0, 1]. In this framework, a visibility scale is an improvement that results in a dynamic transmission map. As a result, the visibility scale, based on mean value measurement, determines an appropriate scattering coefficient.

The scattering parameter β depends on the weather condition as in Table 2. The value of the visual range is specified as the distance at which the apparent contrast between an observer's dark object and the horizon sky is equivalent to an observation threshold of noticeable contrast, which is typically set at 0.02 in light conditions. Specifically, this scattering parameter is obtained from the visible range, $R_{m,}$ via the relation $\beta = -ln(\epsilon)/R_m$ [23, 30]. Then, based on visibility range mapping, the new visibility scale refers to Table 1 to determine the scattering coefficient. Following that, based on the scattering coefficient and depth map parameter, the transmission map estimation in Eq. (2) was derived. Finally, the transmission and air-light values were incorporated into Eq. (3) to produce a dehazed image. Image enhancement, which is contrast stretching, is used in post-processing. The dehazed images are compared to the ground truth image using image quality assessments such as MSE, PSNR, and SSIM [32]. To experiment, the dehazing code was written in MATLAB 2017b and executed on a CPU (Intel i5 7200, 2.5 GHz 8 GB).

4 Haze Simulation Algorithm

In order to evaluate image quality, the synthetic haze image is used for the input image. The ideal image quality value must be achieved between the original image and the dehazed image. As a result, it can aid in the creation of a high-quality, haze-free image. As shown in Table 3, four visibility ranges are applied as a synthetic haze to the ground truth image dataset in this section: 1 km, 2 km, 3 km, and 4 km.

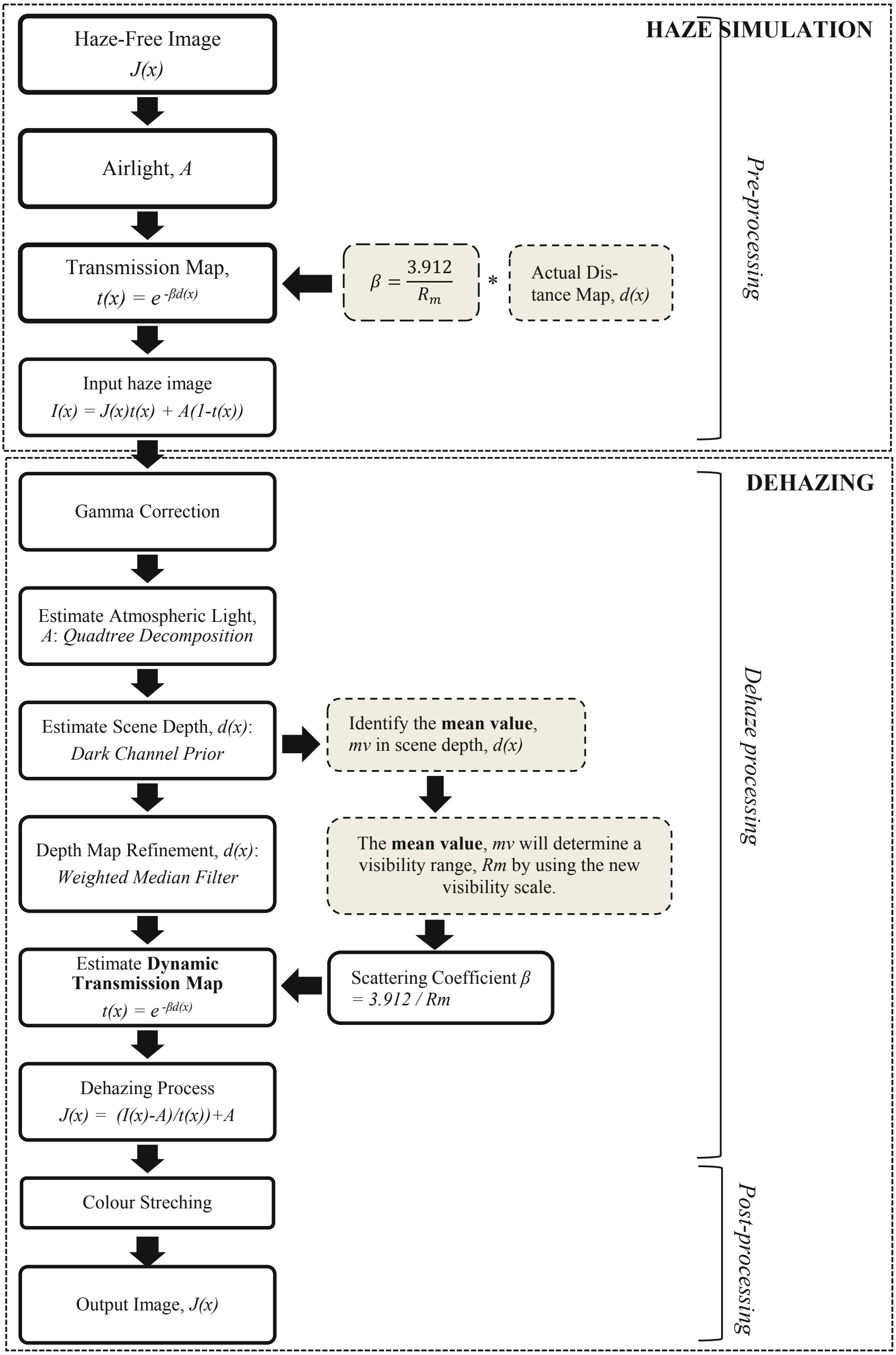

Fig. 2. Haze simulation and dehazing framework

Table 2. The weather conditions visibility range and its scattering coefficient [30]

No.	Weather condition	Visibility range, km	Scattering coefficient, β
1	Dense fog	<50 m	> 78.2
2	Thick fog	50 m–200 m	78.2–19.6
3	Moderate fog	200 m–500 m	19.6–7.82
4	Light fog	500 m–1000 m	7.82–3.91
5	Thin fog/dense haze	1 km–2 km	3.91–1.96
6	Haze	2 km–4 km	1.96–0.954
7	Light haze	4 km–10 km	0.954–0.391
8	Clear	10 km–20 km	0.391–0.196
9	Very clear	20 km–50 km	0.196–0.078
10	Exceptionally clear	>50 km	0.078
11	Pure air	277 km	0.0141

Table 3. The synthetic haze datasets with different four haze levels

Visibility Range, km	**1 Dense haze**	**2 Haze**	**3 Haze**	**4 Light haze**	**Ground Truth**
Dataset					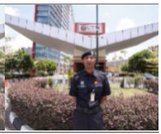

The process of the haze simulation algorithm is summarized as follow:

BEGIN: Input haze-free image: J(x)
Step 1: *Define default airlight value, A = [1,1,1]*
Step 2: *Define a transmission map, t(x)*
Step 3: *Measure scene depth,* $d(x)$ *with Distance Calculator*
for *each haze visibility range,* R_m *[1,2,3,4] in kilometre*
Step 3.1: *define the scattering coefficient,*

$$\beta = \frac{3.912}{R_m}$$

Step 3.2: *calculate the transmission value,* $t(x) = e^{-\beta d(x)}$
Step 3.3: *calculate I(x) = J(x)t(x) + A(1-t(x))*
end
END: Output hazy image: I(x)

The synthetic haze image is used to evaluate the quality of the process by assessing the image quality. The optimal value for the measurement of the image quality between the input and the dehaze image must be achieved. The production of a high-quality, haze-free image can be beneficial. Consequently, with hazy simulation, we proposed a new data set. Air Pollutant Index (API) for government agencies is used in determining or predicting polluted air. An overview of the Malaysian outdoor scene on a clear day that takes into consideration the weather is good and the air pollutants index is good, as shown in Table 4. The API range of 300 to 500 showed a hazardous air quality with a higher environmental and health impact potential. Since each pollutant varies in concentration, API values are grouped into a standardised public health warning [33].

Table 4. Air pollutant index category

Category	Air pollutant index	Visibility range (*MI*)	Visibility range (km)
Good	0–50	>10	>16.1
Moderate	51–100	5–10	8.05–16.1
Unhealthy for sensitive group	101–150	3–5	4.83–8.05
Unhealthy	151–200	1.5–3	2.41–4.83
Very unhealthy	201–300	1	1.61–4.83
Hazardous	300>	<1	<1.61

In order to enhance the efficiency of the dehazing method, various haze conditions provided by Zhang can be demonstrated [23]. Zhang [23] creates five scenarios from light fog to thick fog. The weather affects the scattering parameter. This scattering parameter is calculated from the visible range, R_m, using the relation $\beta = \frac{-ln(\in)}{Rm}$ [30]. The values of these properties simulate hazy images and capture haze-free images with a distance *d(x)* calculated in kilometres (*km*) by the Distance Calculator application, as shown in Fig. 3. The visibility ranges from 1 to 10 km are referred to as simulating a synthetic haze [24]. In this paper, four different haze conditions were used, listed in Table 2: 1 km, 2 km, 3 km, and 4 km.

Based on the features of the haze-free data set in Table 5, the synthetic haze is simulated into four categories based on the haze weather in Table 2. In order to define the transmission map with Eq. (2), We used an actual distance (in kilometres). The transmission was calculated as step 4.2:

$$t(x) = e^{-\beta d(x)}$$

For example,
for 1 km,

$$t(x) = e^{-(3.91)(0.2))} = 0.457$$

Table 5. The properties of haze-free dataset

Venue	UTM KL entrance
Time	Monday, 12 March 2018 1:18 PM
API	22 – Good
Temperature	31 °C - Clouds and Sun
Distance	200 m
Device	Canon EOS 5D Mark III, Lens 17 mm
Dimensions	864 × 576 pixels
Image type	PNG
Properties	ISO 250, Aperture f/4, Shutter Speed 1/1000 s

Fig. 3. The captured clear image and distance measurement with the Distance Calculator application.

for 2 km,

$$t\left(x_{|\beta=1.96|}\right) = e^{-(1.96)(0.2))} = 0.676$$

Step 3.3 is to execute the hazy image using Eq. (1) after the transmission value has been defined as in Eq. (2). As a result, the proposed dehazing algorithm will make use of this haze dataset.

5 Image Dehazing Algorithm

The dehazing algorithm is depicted as a procedure for implementing the dehazing algorithm's enhancement with the dynamic scattering coefficient. To obtain a dehazed image, it was applied to each different synthetic haze dataset, which included light haze, moderate haze, and dense haze.

The proposed Dehazing algorithm

Input haze image: I(x)
Step 1: *Apply Gamma Correction to the input image.*
Step 2: *Estimate airlight, A with Quadtree Decomposition of DCP*
Step 3: *Measure Scene depth with Dark Channel Prior, d(x)*
Step 4: *Refinement depth with Weighted Median Filters*
Step 5: *Define mean value, mv from the known depth information.*
Step 6: *Determine the scattering coefficient value from the R_m visibility scale, $\beta = 3.912 / R_m$*
Step 7: *Estimate transmission, $t(x) = e^{(-\beta * d(x))}$*
Step 8: *Recover the scene radiance, $J(x) = \frac{I(x)-A}{t(x)} + A$*
Step 9: *Post-processing with Contrast Stretching to J(x)*
Output scene radiance: J(x)

5.1 Depth Estimation

Gamma correction was applied to an image input from a simulated synthetic haze image to control its brightness. The quad-tree decomposition algorithm then chooses the sub-block with the highest average value among the four divided blocks. The air-light estimate from the quad-tree subdivision is obtained repeatedly from a grey scaled hazy image up to a predetermined number of times. The air-light can be calculated as the pixel colour vector between pixels in the final selected area with the lowest Euclidean norm. Air light can thus be estimated more precisely by lowering the Euclidean norm [31]. A form of haze-free outdoor image statistics is the dark channel prior [11]. It focuses on a critical observation: most local patches in haze-free outdoor images contain some very low-intensity pixels in at least one colour channel. Using this before the haze imaging model, we can directly estimate the thickness of the haze and retrieve a high-quality haze-free image. The previous dark channel was founded on the following observations from haze-free outdoor images: In most non-sky patches, at least one colour channel has a very low intensity of specific pixels. Because of the additive air-light, a hazy image is brighter than its haze-free counterpart, where transmission is low. As a result, in areas with a denser haze, the dark channel in the hazy image will be more intense. A dark channel is defined as follows:

$$d = \min_{y \in \Omega(x)} \left(\min_{c \in \{r,g,b\}} J^c(y) \right) \tag{4}$$

where J^c is the intensity of a colour channel $c \in \{r, g, b\}$ of an RGB image, and x is a local patch centred on pixel. Then, according to Eq. (4), the dark channel $d(x)$ is chosen as the lowest value among the three-colour channels and all pixels in $\Omega(x)$. Thus, the visual intensity of the dark channel is a rough estimate of the haze thickness [11]. The methods for smoothing the depth map are different from many other techniques for dehazing. The methods of filtration include Gaussian, soft matting, bilateral, and guided filters. In addition, to improve computational efficiency, a weighted median filter [34] is used to refine the rough approximation and smooth the image. In addition, a weighted median filter [34] is used to refine the rough approximation and smooth the image to improve computational effectiveness.

5.2 Dynamic Scattering Coefficient

At Step 7, the dark channel estimates the scene depth, and the transmission map is computed. In the previous method, the scattering coefficient value was typically set to a constant value. However, almost all existing algorithms for single image dehazing are based on constant assumptions, a more flexible model has highly sought after. This paper suggested a new dynamic scattering coefficient, depending on haze thickness for each image. The scattering coefficient will be computed using the mean value and the mv in-depth map estimation. First, we estimated the visibility range, R_m using the mean value, mv, and a visibility scale ranging from 0.5 m to 10 km, based on the meteorological range in Table 2. Then, we divided that range into intensity values (0, 1) and created a visibility scale as follows:

$$\textit{visibility scale range} = \frac{1}{10\,\text{km} - 0.05\,\text{km}} = \frac{1}{9.95\,\text{km}} = 0.1005 \tag{5}$$

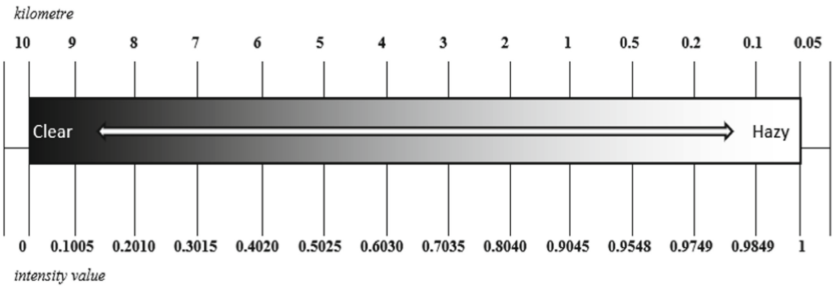

Fig. 4. The proposed new visibility scales to mapping visibility range based on mean values from scene depth intensity.

The example of visibility scale mapping:

if {*mean value*} < 0.1005
  {*visibility range*} = 10;
elseif {*mean value*} < 0.2010
.
.
elseif {*mean value*} < 1
  {*visibility range*} = 0.1;
elseif {*mean value*} >=1
  {*visibility range*} = 0.05;

Table 6. The visibility range to its corresponding scattering coefficient

Visibility range, R_m	Scattering coefficient, β
1	3.9120
2	1.9560
3	1.3040
4	0.9780
5	0.7824
6	0.6520
7	0.5589
8	0.4890
9	0.4347
10	0.3912

The mean values, *mv*, of the depth map intensity must be mapped to this scale to determine the scattering coefficient, as shown in Table 6. The transmission map will be estimated using the scattering coefficient. Because hazy images have varying haze thicknesses, this dynamic scattering coefficient in the dehazing algorithm efficiently produces a better haze-free image. Instead of the constant assumption, this proposed method will set the parameter value based on the depth of the scene. Following transmission estimation, we completed the dehazing process by reversing the atmospheric scattering model in Eq. (3) to obtain a haze-free image. In Fig. 5, we improved the result with image enhancement, which is contrast stretching to increase the image's contrast by extending its range of intensity values through a range of values. Figure 6 depicts the entire dehazing process.

Dehaze image before contrast stretching

Dehaze image after contrast stretching

Fig. 5. A comparison between before and after image enhancement.

6 Image Dehazing Result

This section demonstrates how we used our dehazing method to achieve a haze-free image. The example dataset from a hazy image, scene depth estimation, depth refinement, transmission estimation, dehaze image, and image enhancement are shown in Fig. 6. This process has proven to be effective in removing haze. We proved this method by comparing our results to the ground truth image, as explained in the following section.

(a) (b) (c) (d) (e) (f)

Fig. 6. The steps of the dehazing process (a) Hazy image (b) Scene depth (c) Depth refinement (d) transmission map (e) Dehaze image (f) Image enhancement

7 Benchmark for Comparative Analysis

The main objective of simulating different conditions of haze is to show that the dehazing algorithm can remove haze at all hazy conditions while maintaining image quality. Therefore, the following dehazing methods were compared: Dark Channel Prior [11], Colour Attenuation Prior [17], DehazeNet [18], Haze-Line [19], and Multi-Layer Perceptron [35], respectively. In order to assess the results of such dehazing procedures the Mean-Squared Error (MSE), Peak-Signal-to-Noise Ratio (PSNR), and the Measurement of the Structural Same Index (SSIM), are used [32]. The results of dehazing methods are shown visually in Tables 7 and quantitatively in Table 8.

The Dark Channel Prior method is capable of removing haze at all levels of haze. The sky, on the other hand, appears oversaturated. Colour Attenuation Prior is an efficient way to reduce haze in a light hazy condition while still appearing natural. However, it was not successful in dense haze conditions. The images that resulted are still hazy. The DehazeNet result appears to be ideal for removing haze in all conditions while maintaining quality, especially in dense haze conditions. However, in the hazy light conditions, it was still at a disadvantage compared to CAP. The Haze-Line method result looks are over contrast and unnatural in all conditions. On the other hand, the Multi-Layer Perceptron method removes haze, but it appears to reduce contrast, making the image darker.

Table 7. The result of dehazing method for VHAZE images (a) Hazy Image (b) Dark Channel (c) Colour Attenuation Prior (d) DehazeNet (e) Haze Line (f) Multilayer Perceptron (g) Proposed

	1km	***2km***	***3km***	***4km***
DCP [11]				
CAP [17]				
DN [18]		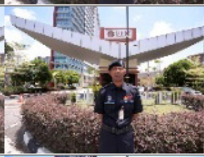		
HL [19]				
MLP [35]				
Proposed				
	R_m = 3 Km, β=1.3040	R_m = 4 Km, β=0.9780	R_m = 4 Km, β=0.9780	R_m = 5 Km, β=0.7824

However, in all hazy levels, our proposed method outperforms the other method in MSE, PSNR, and SSIM. At the MSE value, the difference error between the original and dehazed images is the least. On the other hand, PSNR value is the most better-quality value and at SSIM is a higher value match to the benchmark than others. Furthermore, each level of haze has been estimated with a suitable coefficient to remove haze. This analysis demonstrated that our dehazing method could overcome haze at various haze levels using synthetic haze images and produce optimal quality in the dehazing method.

Table 8. An image quality assessment for first result of dehazing methods

(km)	IQA	DCP [11]	CAP [17]	DN [18]	HL [19]	MLP [35]	Own
1	MSE	0.0071	0.0092	0.0035	0.0191	0.0056	**0.0002**
	PSNR	21.5075	20.3531	24.5885	17.1888	22.4973	**37.5957**
	SSIM	0.9230	0.9339	0.9663	0.8584	0.9540	**0.9964**
2	MSE	0.0101	0.0018	0.0015	0.0199	0.0075	**0.0005**
	PSNR	19.9742	27.3890	28.3691	17.0133	21.2236	**33.1622**
	SSIM	0.9099	0.9751	0.9740	0.8541	0.9493	**0.9936**
3	MSE	0.0111	0.0030	0.0034	0.0240	0.0076	**0.0008**
	PSNR	19.5365	25.2879	24.6757	16.1977	21.2168	**30.7357**
	SSIM	0.9042	0.9667	0.9342	0.8451	0.9449	**0.9901**
4	MSE	0.0117	0.0038	0.0047	0.0307	0.0075	**0.0008**
	PSNR	19.3360	24.1465	23.2813	15.1217	21.2335	**31.1194**
	SSIM	0.9014	0.9590	0.9096	0.8282	0.9417	**0.9878**

The real hazy images shown in Table 9 have been used as a dataset to apply to our dehazing method. These images were captured in Malaysia's outdoor scene with different API values, which consisted of Moderate, Unhealthy and Very Unhealthy conditions. Even these datasets do not provide a haze-free image as a benchmark, but the result shows the capability to remove haze with a suitable scattering coefficient. Table 10 is a dehazing result from a sample dataset in the latest dehazing study. We also applied our dehazing method by using this dataset to prove the efficiency of our method.

The result gives an estimate of the visibility range for each haze image. Our method was successful in removing haze from all haze levels at various haze levels. Furthermore, by determining the appropriate scattering coefficient for each level, the enhancement method contributed to dynamic transmission. This dynamic transmission was successful in reducing issues like over-enhanced and dense haze. Although it produces better results, this enhancement method has limitations when applied to indoor images and images with unreal haze. Even though the proposed dehazing method successfully removed haze and produced a better result, it still requires improvement in the new proposed visibility scaling, as shown in Fig. 4. The visibility range derived from the visibility scale would seem inaccurate in mapping the actual haze image condition.

Table 9. Real-world haze images in Malaysia based on the air pollutant index

Date and Time	7 August 2019 4.26 pm	18 Sept 2019 9.10 am	19 Sept 2019 7.59 am
API	51-100 Moderate (75*)	101-200 Unhealthy (188*)	201-300 Very Unhealthy (271*)
°C	32°C Broken Clouds 6km	28°C Broken clouds 2km	25°C Dense Fog 1km
Range	8-16 km	2-5 km	1-2km
Haze Image			
DCP	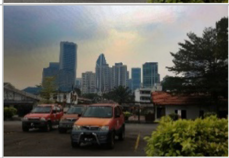	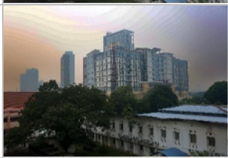	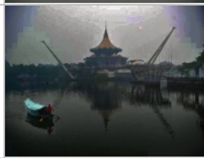
CAP	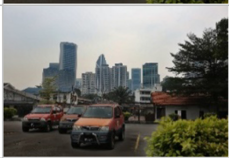	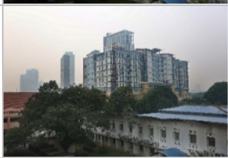	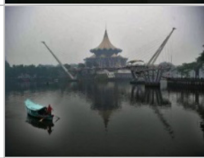
DN	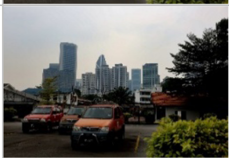		
HL	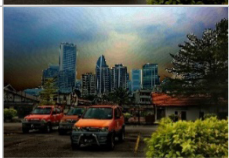	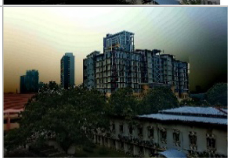	
MLP	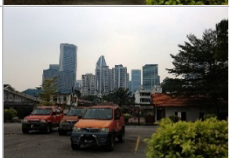		
Own	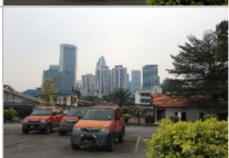 R_m = 5 km, β=0.7824	 R_m = 4 km, β=0.9780	 R_m = 4 km, β=0.9780

Table 10. The result of dehazing method for random hazy images (a) Hazy Image (b) Dark Channel (c) Colour Attenuation Prior (d) DehazeNet (e) Haze Line (f) Multilayer Perceptron (g) Proposed

(a)
(b)
(c)
(d)
(e)
(f)
(g)

R_m = 6 km, $\boldsymbol{\beta}$=0.6520	R_m = 6 km, $\boldsymbol{\beta}$=0.6520	R_m = 5 km, $\boldsymbol{\beta}$=0.7824	R_m = 5 km, $\boldsymbol{\beta}$=0.7824	R_m = 6 km, $\boldsymbol{\beta}$=0.6520

8 Conclusion

Many applications, such as computer vision, surveillance systems, and remote sensing, benefit from the dehazing method. As a result, many dehazing efforts have been made to improve image quality by removing haze. However, the remaining problems are insufficiently recovered from the denser haze or low haze and cause the haze's thickness issues. Therefore, a new synthetic haze was presented in a single image dataset, simulating four different, weather-based hazy conditions. The importance of this experiment is to ensure the efficiency and quality of the dehazing method while removing haze from different haze levels. Furthermore, the results were visually compared to existing state-of-the-art schemes to validate the significance of the proposed technique. As a result, various standard datasets will yield better haze-free images, which will benefit other downstream applications. Furthermore, this approach will be studied by providing a dehazing algorithm that addresses all of the dehazing problems in future research in the visibility scales.

Acknowledgements. This research was funded by the Ministry of Higher Education through the Fundamental Research Grant Scheme and managed by the Research Management Centre (RMC) of Universiti Teknologi Malaysia Vot No. R.K130000.7856.5F036.

References

1. Narasimhan, S.G., Nayar, S.K.: Vision and the atmosphere. Int. J. Comput. Vision **48**(3), 233–254 (2002)
2. Xue, R., Zhong, M., Zhang, E., Zhao, S., Zhang, D.: Real-time image haze removal method for fire scene images. In: 2018 6th International Conference on Machinery, Materials, and Computing Technology (ICMMCT). Atlantis Press (2018)
3. Dong, T., Zhao, G., Wu, J., Ye, Y., Shen, Y.: Efficient traffic video dehazing using adaptive dark channel prior and spatial-temporal correlations. Sensors **19**(7), 1593 (2019)
4. Koschmieder, H.: Theorie der horizontalen sichtweite. In: Beitrage zur Physik der freien Atmosphare (1924)
5. Cozman, F., Krotkov, E.: Depth from scattering. In: Proceedings of IEEE Computer Society Conference on Computer Vision and Pattern Recognition, pp. 801–806, June 1997
6. Narasimhan, S.G., Nayar, S.K.: Contrast restoration of weather degraded images. IEEE Trans. Pattern Anal. Mach. Intell. **25**, 713–724 (2003)
7. Schechner, Y.Y., Narasimhan, S.G., Nayar, S.K.: Polarization-based vision through haze. Appl. Opt. **42**, 511–525 (2003)
8. Kopf, J., et al.: Deep photo: model-based photograph enhancement and viewing. ACM Trans. Graph. **27**, 1–10 (2008). In Siggraph ASIA
9. Tan, R.T.: Visibility in bad weather from a single image. In: IEEE International Conference on Computer Vision and Pattern Recognition, pp. 1–8. IEEE (2008)
10. Fattal, R.: Single image dehazing. ACM Trans. Graph. **27**(3), 72 (2008)
11. He, K., Sun, J., Tang, X.: Single image haze removal using dark channel prior. IEEE Trans. Pattern Anal. Mach. Intell. **33**(12), 1956–1963 (2011)
12. Tarel, J.P., Hautiere, N.: Fast visibility restoration from a single colour or grey level image. In: IEEE International Conference on Computer Vision, pp. 2201–2208. IEEE (2009)
13. Meng, G., Wang, Y., Duan, J., Xiang, S., Pan, C.: Efficient image dehazing with boundary constraint and contextual regularization. In: Proceedings of the IEEE International Conference Computer Vision, Washington, D.C., USA, pp. 617–624 (2013)
14. Ancuti, C.O., Ancuti, C.: Single image dehazing by multi-scale fusion. IEEE Trans. Image Proc. **22**(8), 3271–3282 (2013)

15. Fattal, R.: Dehazing using colour-lines. ACM Trans. Graph. **34**(1), 1–14 (2014)
16. Tang, K., Yang, J., Wang, J.: Investigating haze-relevant features in a learning framework for image dehazing. In: Proceedings of the IEEE Conference Computer Vision Pattern Recognition, Columbus, Ohio, USA, pp. 2995–3002 (2014)
17. Zhu, Q., Mai, J., Shao, L.: A fast single image haze removal algorithm using colour attenuation prior. IEEE Trans. Image Process. **24**(11), 3522–3533 (2015)
18. Cai, B., Xu, X., Jia, K., Qing, C., Tao, D.: DehazeNet: an end-to-end system for single image haze removal. IEEE Trans. Image Process. **25**(11), 5187–5198 (2016)
19. Berman, D., Treibitz, T., Avidan, S.: Non-local image dehazing. In: Proceedings of the IEEE Conference Computer Vision and Pattern Recognition, Las Vegas, Nevada, USA, pp. 1674–1682 (2016)
20. Tarel, J.P., Hautiere, N., Caraffa, L., Cord, A., Halmaoui, H., Gruyer, D.: Vision enhancement in homogeneous and heterogeneous fog. IEEE Intell. Transp. Syst. Mag. **4**(2), 6–20 (2012)
21. Ancuti, C., Ancuti, C.O., Vleeschouwer, C.D.: D-HAZY: a dataset to evaluate quantitatively dehazing algorithms. In: IEEE International Conference on Image Processing, pp. 2226–2230, September 2016
22. El Khoury, J., Thomas, J.-B., Mansouri, A.: A color image database for haze model and dehazing methods evaluation. In: Mansouri, A., Nouboud, F., Chalifour, A., Mammass, D., Meunier, J., ElMoataz, A. (eds.) ICISP 2016. LNCS, vol. 9680, pp. 109–117. Springer, Cham (2016). https://doi.org/10.1007/978-3-319-33618-3_12
23. Zhang, Y., Ding, L., Sharma, G.: HazeRD: an outdoor dataset for dehazing algorithms. In: Proceedings of the IEEE International Conference Image Processing, Beijing, China, pp. 3205–3209 (2017)
24. Ancuti, C.O., Ancuti, C., Timofte, R., De Vleeschouwer. C.: O-HAZE: a dehazing benchmark with real hazy and haze-free outdoor images. In: IEEE/CVF Conference on Computer Vision and Pattern Recognition Workshops (CVPRW) (2018)
25. Ancuti, C.O., Ancuti, C., Timofte, R., De Vleeschouwer, C.: I-HAZE: a dehazing benchmark with real hazy and haze-free indoor images. In: IEEE/CVF Conference on Computer Vision and Pattern Recognition Workshops (CVPRW) (2018)
26. http://vision.middlebury.edu/stereo/data/scenes2014
27. http://cs.nyu.edu/~silberman/datasets/nyudepthv2.html
28. Husain. N.A., Mohd Rahim, M.S., Kari, S., Chaudry, H.: The simulation of synthetic haze based on visibility range for dehazing method in single image. In: 5th International Conference on Engineering and Technology (ICET 2020), Melbourne, Australia, pp. 20–22, March 2020
29. Husain, N.A., Mohd Rahim, M.S., Kari, S., Chaudry, H.: VRHAZE: the simulation of synthetic haze based on visibility range for dehazing method in single image. In: 6th International Conference on Interactive Digital Media (ICIDM 2020), International Virtual Conference, 14–15 December 2020
30. McCartney, E.J.: Optics of the Atmosphere: Scattering by Molecules and Particles. Wiley, New York (1976)
31. Dubok, P., et al.: Single image dehazing with image entropy and information fidelity. In: ICIP, pp. 4037–4041 (2014)
32. Wang, Z.A., Bovik, C., Sheikh, H.R., Simoncelli, E.P.: Image quality assessment: from error visibility to structural similarity. IEEE Trans. Image Process. **13**(4), 600–612 (2004)
33. O'Neil, S.M., Lahm, P.W., Fitch, M.J., Broughton, M.: Summary and analysis of approaches linking visual range, PM2.5 concentrations, and air quality health impact indices for wildfires. J. Air Waste Manag. Assoc. **63**(9), 1083–1090 (2013)
34. Zhang, Q., Xu, L. Jia, J.: 100+ times faster weighted median filter. In: IEEE Conference on Computer Vision and Pattern Recognition (CVPR) (2014)
35. Salazar-Colores, S., Cruz-Aceves, I., Ramos-Arreguin, J.M.: Single image dehazing using a multi-layer perceptron. J. Electron. Imaging **27**(4), 0430 (2018)